5 White DA. The phospholipids composition of mammalian tissues. In: Ansell GB, Hawthorne JN, Dawson RMC, eds. *Form and Function of Phospholipids*. Amsterdam: Elsevier, 1973; 441–82.
6 Bishop WR, Bell RM. Assembly of phospholipids into cellular membranes: biosynthesis, transmembrane movement and intracellular translocation. *Annu Rev Cell Biol* 1988; **4**: 579–610.
7 Shindou H, Hishikawa D, Harayama T, Yuki K, Shimizu T. Recent progress on acyl CoA: lysophospholipid acyltransferase research. *J Lipid Res* 2009; **50**(Suppl.): S46–51.
8 Mansilla F, da Costa KA, Wang S *et al.* Lysophosphatidylcholine acyltransferase 1 (LPCAT1) overexpression in human colorectal cancer. *J Mol Med (Berl)* 2009; **87**: 85–97.
9 Woods AS, Jackson SN. Brain tissue lipidomics: direct probing using matrix-assisted laser desorption/ionization mass spectrometry. *AAPS J* 2006; **8**: E391–5.
10 McDonnell LA, Heeren RM. Imaging mass spectrometry. *Mass Spectrom Rev* 2007; **26**: 606–43.
11 Chaurand P, Sanders ME, Jensen RA, Caprioli RM. Proteomics in diagnostic pathology: profiling and imaging proteins directly in tissue sections. *Am J Pathol* 2004; **165**: 1057–68.
12 Cornett DS, Reyzer ML, Chaurand P, Caprioli RM. MALDI imaging mass spectrometry: molecular snapshots of biochemical systems. *Nat Methods* 2007; **4**: 828–33.
13 Seeley EH, Caprioli RM. Molecular imaging of proteins in tissues by mass spectrometry. *Proc Natl Acad Sci U S A* 2008; **105**: 18126–31.
14 Cazares LH, Troyer D, Mendrinos S *et al.* Imaging mass spectrometry of a specific fragment of mitogen-activated protein kinase/extracellular signal-regulated kinase kinase kinase 2 discriminates cancer from uninvolved prostate tissue. *Clin Cancer Res* 2009; **15**: 5541–51.
15 Morita Y, Ikegami K, Goto-Inoue N *et al.* Imaging mass spectrometry of gastric carcinoma in formalin-fixed paraffin-embedded tissue microarray. *Cancer Sci* 2010; **101**: 267–73.
16 Liu Y, Chen Y, Momin A *et al.* Elevation of sulfatides in ovarian cancer: an integrated transcriptomic and lipidomic analysis including tissue-imaging mass spectrometry. *Mol Cancer* 2010; **9**: 186.
17 Harada T, Yuba-Kubo A, Sugiura Y *et al.* Visualization of volatile substances in different organelles with an atmospheric-pressure mass microscope. *Anal Chem* 2009; **81**: 9153–7.
18 Kurabe N, Hayasaka T, Igarashi H *et al.* Visualization of phosphatidylcholine (16:0/16:0) in type II alveolar epithelial cells in the human lung using imaging mass spectrometry. *Pathol Int* 2013; **63**: 195–200.
19 Shimma S, Sugiura Y, Hayasaka T, Zaima N, Matsumoto M, Setou M. Mass imaging and identification of biomolecules with MALDI-QIT-TOF-based system. *Anal Chem* 2008; **80**: 878–85.
20 Deininger SO, Ebert MP, Futterer A, Gerhard M, Rocken C. MALDI imaging combined with hierarchical clustering as a new tool for the interpretation of complex human cancers. *J Proteome Res* 2008; **7**: 5230–6.
21 Willems SM, van Remoortere A, van Zeijl R, Deelder AM, McDonnell LA, Hogendoorn PC. Imaging mass spectrometry of myxoid sarcomas identifies proteins and lipids specific to tumour type and grade, and reveals biochemical intratumour heterogeneity. *J Pathol* 2010; **222**: 400–9.
22 Kahyo T, Iwaizumi M, Shinmura K *et al.* A novel tumor-derived SGOL1 variant causes abnormal mitosis and unstable chromatid cohesion. *Oncogene* 2011; **30**: 4453–63.
23 Sugimura H, Mori H, Nagura K *et al.* Fluorescence in situ hybridization analysis with a tissue microarray: 'FISH and chips' analysis of pathology archives. *Pathol Int* 2010; **60**: 543–50.
24 Okudela K, Yazawa T, Ishii J *et al.* Down-regulation of FXYD3 expression in human lung cancers: its mechanism and potential role in carcinogenesis. *Am J Pathol* 2009; **175**: 2646–56.
25 Costa WH, Rocha RM, Cunha IW, Guimaraes GC, Zequi Sde C. Immunohistochemical expression of CD44s in renal cell carcinoma lacks independent prognostic significance. *Int Braz J Urol* 2012; **38**: 456–65.
26 Natsume H, Shinmura K, Tao H *et al.* The CRKL gene encoding an adaptor protein is amplified, overexpressed, and a possible therapeutic target in gastric cancer. *J Transl Med* 2012; **10**: 97.
27 Garrett TJ, Yost RA. Analysis of intact tissue by intermediate-pressure MALDI on a linear ion trap mass spectrometer. *Anal Chem* 2006; **78**: 2465–9.
28 Hayasaka T, Goto-Inoue N, Sugiura Y *et al.* Matrix-assisted laser desorption /ionization quadrupole ion trap time-of-flight (MALDI-QIT-TOF)-based imaging mass spectrometry reveals a layered distribution of phospholipid molecular species in the mouse retina. *Rapid Commun Mass Spectrom* 2008; **22**: 3415–26.
29 Al-Saad KA, Siems WF, Hill HH, Zabrouskov V, Knowles NR. Structural analysis of phosphatidylcholines by post-source decay matrix-assisted laser desorption/ionization time-of-flight mass spectrometry. *J Am Soc Mass Spectrom* 2003; **14**: 373–82.
30 Chen X, Hyatt BA, Mucenski ML, Mason RJ, Shannon JM. Identification and characterization of a lysophosphatidylcholine acyltransferase in alveolar type II cells. *Proc Natl Acad Sci U S A* 2006; **103**: 11724–9.
31 Shindou H, Hishikawa D, Nakanishi H *et al.* A single enzyme catalyzes both platelet-activating factor production and membrane biogenesis of inflammatory cells. Cloning and characterization of acetyl-CoA:LYSO-PAF acetyltransferase. *J Biol Chem* 2007; **282**: 6532–9.
32 Zhao Y, Chen YQ, Bonacci TM *et al.* Identification and characterization of a major liver lysophosphatidylcholine acyltransferase. *J Biol Chem* 2008; **283**: 8258–65.
33 Hishikawa D, Shindou H, Kobayashi S, Nakanishi H, Taguchi R, Shimizu T. Discovery of a lysophospholipid acyltransferase family essential for membrane asymmetry and diversity. *Proc Natl Acad Sci U S A* 2008; **105**: 2830–5.
34 Gijon MA, Riekhof WR, Zarini S, Murphy RC, Voelker DR. Lysophospholipid acyltransferases and arachidonate recycling in human neutrophils. *J Biol Chem* 2008; **283**: 30235–45.
35 Hayasaka T, Goto-Inoue N, Ushijima M *et al.* Development of imaging mass spectrometry (IMS) dataset extractor software. IMS convolution. *Anal Bioanal Chem* 2011; **401**: 183–93.
36 Setou M. *Imaging Mass Spectrometry: Protocols for Mass Microscopy*, 1st edn. Tokyo, Japan: Springer, 2010.
37 Setou M, Kurabe N. Mass microscopy: high-resolution imaging mass spectrometry. *J Electron Microsc (Tokyo)* 2011; **60**: 47–56.
38 Jain S, Zhang X, Khandelwal PJ, Saunders AJ, Cummings BS, Oelkers P. Characterization of human lysophospholipid acyltransferase 3. *J Lipid Res* 2009; **50**: 1563–70.

Supporting Information

Additional Supporting Information may be found in the online version of this article:

Fig. S1. Involvement of LPCAT4 in the synthesis of PC(16:0/16:1) in DLD1 *in vitro*.

Fig. S2. Immunohistochemical analysis of the expression of LPCAT4 in adenomatous polyp.

Table S1. Clinicopathological profile of the cases on tissue microarray.

Table S2. Clinicopathological profile of polyps.

Table S3. Correlation of intensities generated using a mass microscope and immunohistochemical score.

Supplementary Methods. Including: LPCAT assay; immunohistochemistry; RNAi; and RT-PCR.

doi: 10.1111/cas.12221

Pathology International

Pathology International 2013; **63**: 195–200 doi:10.1111/pin.12050

Rapid Communication

Visualization of phosphatidylcholine (16:0/16:0) in type II alveolar epithelial cells in the human lung using imaging mass spectrometry

Nobuya Kurabe,[1] Takahiro Hayasaka,[2] Hisaki Igarashi,[1] Hiroki Mori,[5] Keigo Sekihara,[3] Hong Tao,[1] Hidetaka Yamada,[1] Tomoaki Kahyo,[1] Ippei Onishi,[1] Hiroe Tsukui,[1] Akikazu Kawase,[3] Shun Matsuura,[1,4] Yusuke Inoue,[1,4] Kazuya Shinmura,[1] Kazuhito Funai,[3] Mitsutoshi Setou[2] and Haruhiko Sugimura[1]

Departments of [1]Tumor Pathology, [2]Cell Biology and Anatomy, [3]Surgery I and [4]Internal Medicine II, Hamamatsu University School of Medicine, and [5]Department of Pathology, Hamamatsu Medical Center, Hamamatsu, Shizuoka, Japan

Imaging mass spectrometry (MS) is an emerging technique that can detect numerous biomolecular distributions in a non-targeting manner. In the present study, we applied a mass imaging modality, mass microscopy, to human lung tissue and identified several molecules including surfactant constituents in a specific structure of the lung alveoli. Four peaks were identified using imaging MS, and the ion at *m/z* 772.5, in particular, was localized at some spots in the alveolar walls. Using an MS/MS analysis, the ion was identified as phosphatidylcholine (PC)(16:0/16:0), which is the main component of lung surfactant. In a larger magnification of the lung specimen, PC (16:0/16:0) was distributed in a mottled fashion in a section of the lung. Importantly, the distribution of PC (16:0/16:0) was identical to that of anti-SLC34A2 antibody immunoreactivity, which is known to be a specific marker of type II alveolar epithelial cells, in the same section. Our experience suggests that imaging MS has excellent potential in human pathology research.

Key words: imaging mass spectrometry, mass microscope, phosphatidylcholine, pulmonary surfactant, SLC34A2

Pulmonary alveoli are mainly composed of two cell types: alveolar type I epithelial cells cover 95% of the surface of alveoli, while alveolar type II epithelial cells secrete pulmonary surfactant. Pulmonary surfactant is a lipoprotein, consisting of disaturated phosphatidylcholine (PC) and various surfactant proteins (SP-A, SP-B, SP-C and SP-D). The main role of lung surfactant is to reduce the tension of alveoli. The impairment of lung surfactant production causes severe respiratory failure in both children and adults with diseases such as respiratory distress syndrome.[1–3] As for surfactant protein, for example, the deletion of the SP-A gene is associated with the prognosis of patients with non-small cell lung cancer.[4] While studies of lipids in lung surfactant using pulmonary broncho-alveolar lavage fluid (BALF) or lung homogenate have been reported,[5,6] imaging studies are scarce; thus, the reality of pulmonary alveoli surfactant *in situ* remains unclear. Direct imaging mass spectrometry (MS) is a newly developed technique. The equipment used for imaging MS consists of a microscopic and mass spectrometric apparatus. Through two-dimensional scanning with a laser on the sample section, this technique enables us to visualize the localization of molecules under atmospheric conditions.[7] For the last decade, this technique has been applied to imaging and discovery tools, such as cancer-specific protein markers and tissue specific biomolecules.[8,9] Morita *et al.* demonstrated that histone H4 was highly expressed in poorly differentiated gastric carcinoma by scanning the tissue microarray (TMA) of formalin-fixed paraffin-embedded (FFPE) specimens by imaging MS.[8] Shimma *et al.* reported that imaging MS enabled the visualization and identification of phospholipis, glycolipid and tryptic-digested proteins in the mouse cerebellum specimens.[10] On the other hand, no tools have been available, until recently, for the detection or survey of lipid molecules in tissues. Actually, the generation of antibodies against lipids remains difficult even today, and genetic approaches are often not applicable to the study of lipids. Consequently, visualizing lipids has long been a great challenge for researchers. Recently, lipid imaging has gained popularity as a research tool for investigating lipids in various

Correspondence: Haruhiko Sugimura, MD, PhD, Department of Tumor Pathology, Hamamatsu University School of Medicine, 1-20-1 Handayama, Higashi Ward, Hamamatsu, Shizuoka 431-3192, Japan. Email: hsugimur@hama-med.ac.jp

The authors have no conflicts of interest to declare.

Received 5 December 2012. Accepted for publication 3 April 2013.

fields, since many scientists have noticed that the currently available imaging MS is especially powerful and feasible for detecting a wide range of biomolecules, including lipids.

To clarify the precise localization of surfactant lipid in normal alveoli, we used imaging MS to profile the lipid distribution of pulmonary surfactant. This study successfully identified, for the first time, the distribution of lipids in alveoli using imaging MS.

MATERIALS AND METHODS

Sample preparation

Three lung and one bronchial samples were retrieved from the archives of the Hamamatsu University Hospital. Non-diseased portions of the lung obtained from lung surgical specimens and autopsy specimens were snap-frozen in liquid nitrogen and stored at −80°C until required. Before sectioning, the frozen tissue blocks were left for 30 min at −20°C. The tissue sections were then cut to a thickness of 8 μm at −20°C using a cryostat (CM1950; Leica, Microsystems, Wetzlar, Germany). The tissue sections were stained with hematoxylin and eosin (HE) to identify the pulmonary alveoli. The adjacent sections were transferred onto indium-tin-oxide (ITO)-coated slide glasses (Bruker Daltonics, Billerica, MA, USA) and thawed. The tissue sections were then slowly brought to room temperature and uniformly coated with 2,5-dihydroxybenzoic acid (DHB; Bruker Daltonics) in 70% methanol and 10 mM potassium acetate using a 0.2-mm nozzle airbrush (Procon Boy FWA Platinum; Mr Hobby, Tokyo, Japan).[11]

Imaging MS analysis

All imaging MS analyses were performed using atmospheric pressure (AP)-matrix assisted laser desorption ionization (MALDI) with a quadrupole ion trap (QIT)-time of flight (TOF) analyzer instrument: a mass microscope equipped with a diode-pumped 355-nm Nd:YAG laser (Shimadzu, Kyoto, Japan).[12] All the mass spectra were acquired using mass microscope System software (Shimadzu). The sample was irradiated with a focused laser beam in synchrony with the stage scanning. The mass spectrum was then acquired for each spot on the tissue section. In this manner, ion images showing the distribution of biomolecules within the samples were obtained. The measurements were performed in reflectron mode within a mass range of *m/z* 700–850 using a scan pitch of 7.5 μm (for ×20 magnification) or 20 μm (for ×2.5 magnification) pixel size. The laser shot number and frequency were 200 per pixel and 1000 Hz, respectively. Lipid peak assignments were made by comparing the peak's mass measurement with the LIPID MAPS database (http://lipidmaps.org) and were confirmed using an MS/MS analysis (QSTAR Elite; Applied Biosystems, Foster City, CA, USA). Image reconstruction was performed using the software BioMap (freeware: http://www.maldi-msi.org).[10]

Immunohistochemistry

Tissue preparation and immunohistochemical analyses of the lung specimens were performed as previously described.[13] Following the measurements, the matrix was removed with 70% ethanol and the sections were stained using immunohistochemistry. After matrix removal, the sections were immersed in a 0.3% hydrogen peroxide solution to inhibit endogenous peroxidase activity. For antigen retrieval, the slides were heated at 96°C for 30 min in TE buffer (pH 9.0), followed by incubation at room temperature for 30 min. Affinity-isolated rabbit anti-SLC34A2 antibody (1:500; Sigma, St. Louis, MO, USA) was used. Next, the sections were treated with a peroxidase-conjugated secondary antibody (Histofine Simple Stain MAX PO; Nichirei, Japan) followed by incubation at room temperature for 30 min. For color reactions, the sections were incubated with diaminobenzidine (DAB) Substrate-Chromogen Solution (DAKO Cytomation; Carpinteria, CA, USA) and the sections were counterstained with 0.1% hematoxylin. Following immunohistochemistry, the sections were photographed using Keyence BZ-9000 (Keyence, Tokyo, Japan). The stained sections were co-registered with the imaging MS results and were evaluated histologically by performing a conventional histopathological analysis.

Ethical considerations

The study protocol was approved by the Institutional Review Board of Hamamatsu University School of Medicine (approval 23–91).

RESULTS

To profile the lipid contents in the lung specimen directly, we performed imaging MS. The region of interest (ROI) in the lung specimens was determined based on the ordinary morphology revealed by HE staining (Fig. 1a). Figure 1(b) shows a representative mass spectrum for a lung specimen with four intense peaks (*m/z* 716.0, 737.0, 772.5 and 817.0). The *m/z* range from 700 to 850 was shown to be that of phosphatidylcholine,[14] which is a component of lung surfactant. Of the four peaks shown in Fig. 1(b), the most intense peak was the ion at *m/z* 772.5. To visualize the distribution of ion peaks,

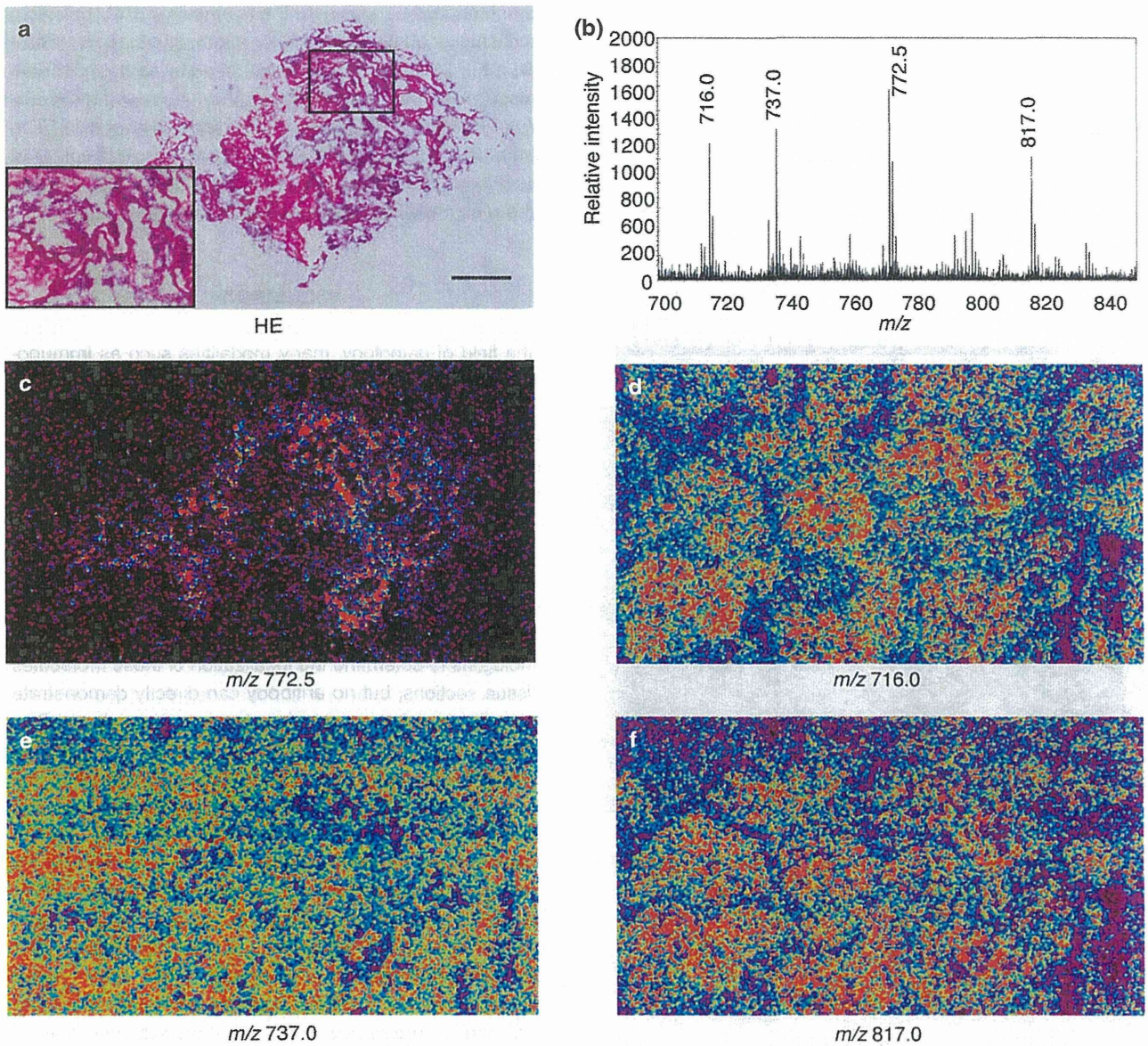

Figure 1 Imaging MS (mass spectrometry) analysis of a lung specimen. (**a**) HE (hematoxylin and eosin) staining of the lung specimen. Scale bar, 500 μm. inset, magnified view of the lung specimen. (**b**) Representative spectra obtained from the lung specimen. The ion at *m/z* 772.5 (**c**), 716.0 (**d**), 737.0 (**e**), and 817.0 (**f**) were imaged using BioMap.

we imported the spectrum data into the imaging software BioMap. Figure 1(c) shows that the peak at *m/z* 772.5 was specifically localized within the lung specimen, while the remaining three peaks were uniformly distributed throughout the entire section (Fig. 1d–f). To identify the ion at *m/z* 772.5, we performed an MS/MS analysis. Figure 2(a) show the MS/MS spectrum obtained from normal lung specimens. LIPID MAPS was used as a reference. The ion at *m/z* 772.5 was assigned as [PC(16:0/16:0) + K^+] because neutral losses of 59 Da and 183 Da were observed, which is indicative of PC. The peak at *m/z* 163 corresponded to cyclophosphate (124 Da) and a potassium ion (39 Da). As shown in Fig. 2(b), PC(16:0/16:0) exhibited a spotty pattern on the alveolar wall when examined at a higher magnification. To specify the PC(16:0/16:0) localization more precisely, we performed an immunohistochemical analysis using an anti-SLC34A2 (solute carrier family 34 (sodium phosphate), member 2) antibody (Fig. 2b). SLC34A2 is specifically expressed in type II alveolar epithelial cells and is formally referred to as sodium-dependent phosphate transporter type IIb (NPT2b) in mice and NaPi-3b in human.[15–18] The PC(16:0/16:0) signal was colocalized with the SLC34A2 antibody

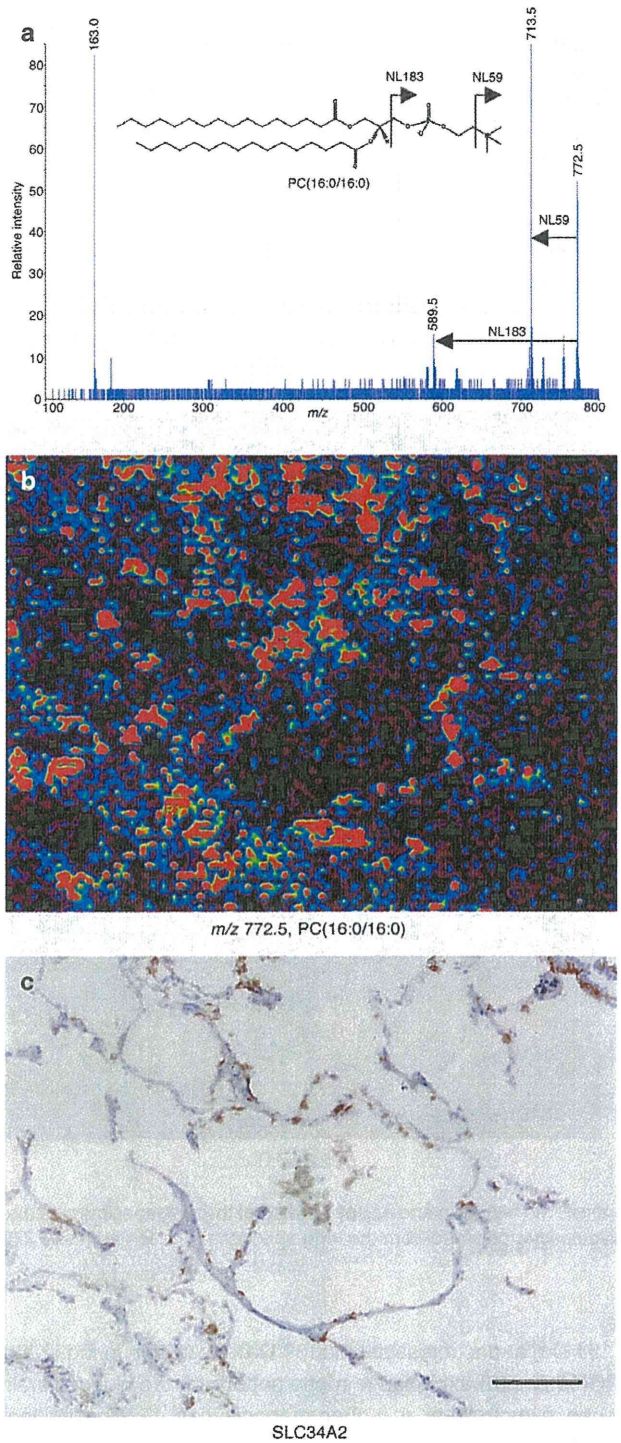

Figure 2 Ion assignment of *m/z* 772.5 and immunohistochemical analysis of a lung specimen. (**a**) An MS/MS analysis was performed to identify the ion at *m/z* 772.5. PC (phosphatidylcholine) (16:0/16:0) signals (**b**) were colocalized with the SLC34A2 antibody immunoreactivity (**c**). Scale bar, 100 μm.

immunoreactivity, suggesting the synthesis of PC(16:0/16:0) in the lamellar bodies of type II alveolar epithelial cells. Moreover, the PC(16:0/16:0) (Fig. 3a,d) signal was not observed in mass spectrum of bronchial specimen, revealing the specificity of PC(16:0/16:0) signal in alveolar epithelial cells. The peak at *m/z* 782.5, was localized at the bronchial epithelial cells (Fig. 3f) and the peaks at *m/z* 737.5 and 775.5, existed in the region without bronchial specimen (Fig. 3c,e).

DISCUSSION

In the field of pathology, many modalities such as immunohistochemistry using several modifications,[3] fluorescence *in situ* hybridization,[19,20] chromogenic *in situ* hybridizaition,[21] microRNA analysis,[22] and, finally, the comprehensive application of state-of-the-art genomic methods[23] are presently being used. Some of these technologies are already used in daily practice, while the future applications of others are being considered. The above-mentioned technologies, however, are still not completely satisfactory for the present needs of pathologists for reasons other than their cost alone. For example, antibodies against known molecules enable pathologists to determine the localization of these molecules in tissue sections, but no antibody can directly demonstrate the localization of an unknown molecule in a specimen. Furthermore, almost no antibodies are available for the detection of lipid molecules, which are important constituents of the human body. Thus, the development of techniques to detect the distributions of unknown molecules accurately is needed. MS and imaging MS have emerged as a useful option for the diagnosis and identification of unknown biomolecules. We previously reported the feasibility of imaging MS in various biological fields.[24–26] In the present study, we focused on the distribution of PC in pulmonary surfactant. PC is composed of many combinations of lipids and can be defined based on the length and degree of acyl chain satiation. We were able to detect the lipid species of PC successfully (Fig. 1). To date, other studies of BALF have provided limited information about the localization of lung surfactant lipid, however, the actual localization of lung surfactant lipid has never been observed. The present study demonstrated that the distribution of lipid surfactant PC(16:0/16:0) corresponded exactly with the distribution of type II alveolar epithelial cells, and we were able to demonstrate the luminal distribution of pulmonary surfactant (Figs 2,3).

In conclusion, to the best of our knowledge, this report is the first to present actual images of the distribution of pulmonary surfactant in alveoli. Our findings should pave the way to further applications of imaging MS in the investigation of lung pathophysiology related to lung surfactant and the function of surfactant in processes such as pulmonary proteinosis, pulmonary microlithiasis, acute respiratory distress syndrome in

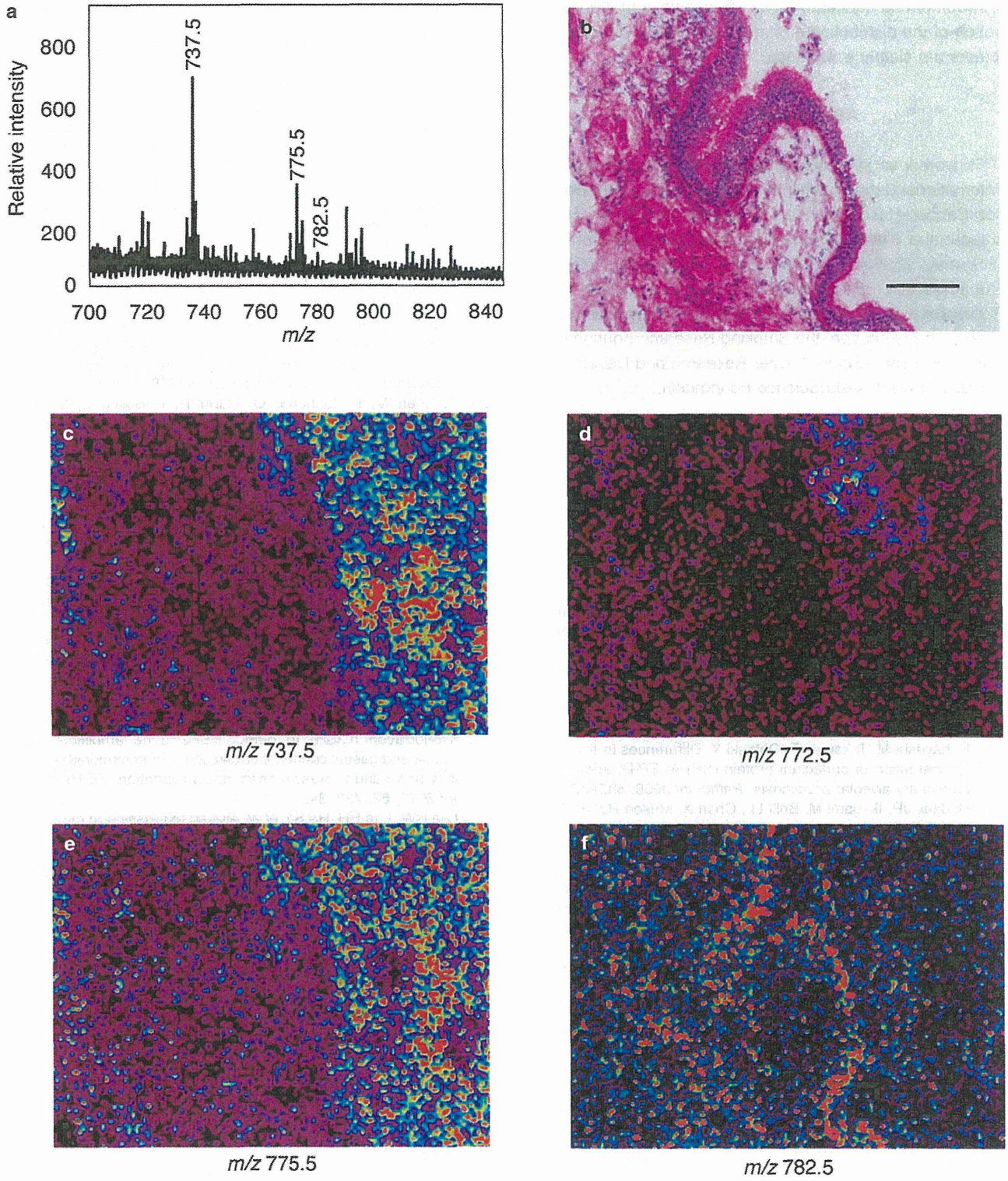

Figure 3 Imaging MS analysis of a bronchial specimen. (**a**) Representative spectra obtained from the bronchial specimen. (**b**) HE (hematoxylin and eosin) staining of the bronchial region. Scale bar, 100 μm. The ion at *m/z* 737.5 (**c**), 772.5 (**d**), 775.5 (**e**), and 782.5 (**f**) were imaged using BioMap.

newborns, and cancer. Further MS analyses of the deterioration of the distribution of surfactant in these diseases and others are clearly warranted.

ACKNOWLEDGMENTS

This work was supported by Grants-in-Aids (Research on International Cooperation in Medical Science, Grants-in-Aids for Cancer Research, 21-1) from the Ministry of Health, Labour and Welfare, the Japan Society for the Promotion of Science (22590356, 22790378, 23116510 and 20670004), the Ministry of Education, Culture, Sports, Science and Technology (221S0001), the Princess Takamatsu Cancer Research Foundation, the Smoking Research Foundation of Japan, National Cancer Center Research and Development Fund, and the Takeda Science Foundation.

REFERENCES

1 Farrell PM, Avery ME. Hyaline membrane disease. *Am Rev Respir Dis* 1975; **111**: 657–88.
2 Petty TL, Silvers GW, Paul GW, Stanford RE. Abnormalities in lung elastic properties and surfactant function in adult respiratory distress syndrome. *Chest* 1979; **75**: 571–4.
3 Pison U, Seeger W, Buchhorn R *et al.* Surfactant abnormalities in patients with respiratory failure after multiple trauma. *Am Rev Respir Dis* 1989; **140**: 1033–9.
4 Jiang F, Caraway NP, Nebiyou Bekele B *et al.* Surfactant protein A gene deletion and prognostics for patients with stage I non-small cell lung cancer. *Clin Cancer Res* 2005; **11**: 5417–24.
5 Kobayashi M, Takeuchi T, Ohtsuki Y. Differences in the immunolocalization of surfactant protein (SP)-A: SP-D, and KL-6 in pulmonary alveolar proteinosis. *Pathol Int* 2008; **58**: 203–7.
6 Bridges JP, Ikegami M, Brilli LL, Chen X, Mason RJ, Shannon JM. LPCAT1 regulates surfactant phospholipid synthesis and is required for transitioning to air breathing in mice. *J Clin Invest* 2010; **120**: 1736–48.
7 Kakimoto Y, Tsuruyama T, Yamamoto T *et al.* Novel in situ pretreatment method for significantly enhancing the signal in MALDI-TOF MS of formalin-fixed paraffin-embedded tissue sections. *PLoS One* 2012; **7**: e41607.
8 Cazares LH, Troyer D, Mendrinos S *et al.* Imaging mass spectrometry of a specific fragment of mitogen-activated protein kinase/extracellular signal-regulated kinase kinase kinase 2 discriminates cancer from uninvolved prostate tissue. *Clin Cancer Res* 2009; **15**: 5541–51.
9 Morita Y, Ikegami K, Goto-Inoue N *et al.* Imaging mass spectrometry of gastric carcinoma in formalin-fixed paraffin-embedded tissue microarray. *Cancer Sci* 2010; **101**: 267–73.
10 Shimma S, Sugiura Y, Hayasaka T, Zaima N, Matsumoto M, Setou M. Mass imaging and identification of biomolecules with MALDI-QIT-TOF-based system. *Anal Chem* 2008; **80**: 878–85.
11 Sugiura Y, Setou M. Selective imaging of positively charged polar and nonpolar lipids by optimizing matrix solution composition. *Rapid Commun Mass Spectrom* 2009; **23**: 3269–78.
12 Harada T, Yuba-Kubo A, Sugiura Y *et al.* Visualization of volatile substances in different organelles with an atmospheric-pressure mass microscope. *Anal Chem* 2009; **81**: 9153–7.
13 Igarashi H, Sugimura H, Maruyama K *et al.* Alteration of immunoreactivity by hydrated autoclaving, microwave treatment, and simple heating of paraffin-embedded tissue sections. *APMIS* 1994; **102**: 295–307.
14 Garrett TJ, Yost RA. Analysis of intact tissue by intermediate-pressure MALDI on a linear ion trap mass spectrometer. *Anal Chem* 2006; **78**: 2465–9.
15 Feild JA, Zhang L, Brun KA, Brooks DP, Edwards RM. Cloning and functional characterization of a sodium-dependent phosphate transporter expressed in human lung and small intestine. *Biochem Biophys Res Commun* 1999; **258**: 578–82.
16 Traebert M, Hattenhauer O, Murer H, Kaissling B, Biber J. Expression of type II Na-P(i) cotransporter in alveolar type II cells. *Am J Physiol* 1999; **277**: L868–73.
17 Hashimoto M, Wang DY, Kamo T *et al.* Isolation and localization of type IIb Na/Pi cotransporter in the developing rat lung. *Am J Pathol* 2000; **157**: 21–7.
18 Huqun, Izumi S, Miyazawa H *et al.* Mutations in the SLC34A2 gene are associated with pulmonary alveolar microlithiasis. *Am J Respir Crit Care Med* 2007; **175**: 263–8.
19 Sugimura H, Mori H, Nagura K *et al.* Fluorescence in situ hybridization analysis with a tissue microarray: 'FISH and chips' analysis of pathology archives. *Pathol Int* 2010; **60**: 543–50.
20 Sugimura H. Detection of chromosome changes in pathology archives: An application of microwave-assisted fluorescence in situ hybridization to human carcinogenesis studies. *Carcinogenesis* 2008; **29**: 681–7.
21 Kiyose S, Igarashi H, Nagura K *et al.* Chromogenic in situ hybridization (CISH) to detect HER2 gene amplification in breast and gastric cancer: Comparison with immunohistochemistry (IHC) and fluorescence in situ hybridization (FISH). *Pathol Int* 2012; **62**: 728–34.
22 Lee HW, Lee EH, Ha SY *et al.* Altered expression of microRNA miR-21, miR-155, and let-7a and their roles in pulmonary neuroendocrine tumors. *Pathol Int* 2012; **62**: 583–91.
23 Shibata T. Cancer genomics and pathology: All Together Now. *Pathol Int* 2012; **62**: 647–59.
24 Hayasaka T, Goto-Inoue N, Ushijima M *et al.* Development of imaging mass spectrometry (IMS) dataset extractor software, IMS convolution. *Anal Bioanal Chem* 2011; **401**: 183–93.
25 Setou M. *Imaging Mass Spectrometry: Protocols for Mass Microscopy*, 1st edn. New York: Springer, 2010.
26 Setou M, Kurabe N. Mass microscopy: High-resolution imaging mass spectrometry. *J Electron Microsc (Tokyo)* 2011; **60**: 47–56.

Genes to Cells

Establishment and characterization of a mutagenized cell line exhibiting the 'cell-in-cell' phenotype at a high frequency

Tomoaki Kahyo* and Haruhiko Sugimura

Department of Tumor Pathology, Hamamatsu University School of Medicine, 1-20-1 Handayama, Higashi-ku, Hamamatsu 431-3192, Japan

Cell-in-cell structures represent live cell events in which one cell internalizes another. Because formation of cell-in-cell structures is a rare event in most cell types and the event is associated with cell death, there has been limited clarification of this phenomenon, and its physiological role and molecular mechanism are yet to be precisely elucidated. In this study, we established a mutagenized cell line that exhibited cell-in-cell structures at a more than 10-fold higher frequency as compared to the parent cells. Interestingly, both engulfment and invasion were increased in the mutagenized cell line as compared with that in the parent cell line in the suspension culture condition. This finding indicates that this mutagenized cell line showed an interchangeable status in terms of its ability to form cell-in-cell structures, and the system described here could be useful for elucidation of the mechanisms regulating the formation of cell-in-cell structures, including engulfment and invasion, in a given cellular environment. Further studies using this cell line are warranted to understand the mechanism of formation and biological significance of the cell-in-cell formation.

Introduction

Cell-in-cell structures, with nested doll-like features, were referred to as 'bird's eye' more than a century ago (Bauchwitz 1981) and have been observed to involve various cell types (Overholtzer & Brugge 2008), including neutrophils in megakaryocytes (Lee 1989; Schmitt *et al.* 2000; Woulfe *et al.* 2008) and thymocytes in thymic nurse cells (Wekerle & Ketelsen 1980; Ritter *et al.* 1981; Martinez *et al.* 2007). Cell-in-cell interactions between these cells are often referred to as emperipolesis, which is a term used to describe the long-term movements of internalized cells (Humble *et al.* 1956) and has often been observed in Rosai–Dorfman disease, a rare, but well-defined histiocytic proliferative disorder (Iyer *et al.* 2009). As described by Humble *et al.*, in emperipolesis, the internalized cells often seem to be wandering around inside the host cells; therefore, emperipolesis is regarded as an event in which the targeted cells are alive and not dead, in contrast to phagocytosis, in which the engulfed cells are usually dead and pathogenic (Takeda & Akira 2001; Krysko & Vandenabeele 2010); however, the term 'emperipolesis' has sometimes been used to represent phagocytosis.

In addition to emperipolesis, the terms 'cell cannibalism' and 'entosis' have also been used to describe cell-in-cell structures. Cell cannibalism has been recognized mostly as an active engulfment event of host cancer cells (Brouwer *et al.* 1984). In contrast, entosis seems to be an event where a cell invades another cell more actively (Overholtzer *et al.* 2007). Cell-in-cell structures have also been observed in various tumors, including breast carcinoma, lung small-cell carcinoma and melanoma (Overholtzer & Brugge 2008), and have been suggested to be involved in the aggressiveness of the malignancy, although the pathological roles of cell-in-cell events in tumor biology remain unclear (Sharma & Dey 2011).

In cell-in-cell events, the host cells can internalize multiple cells (Steinhaus 1981) and also another host cell with an internalized cell (Overholtzer *et al.* 2007). Furthermore, an internalized cell can divide into two daughter cells even inside the host cell and also come out of the host cell (Overholtzer *et al.*

Communicated by: Yusaku Nakabeppu
**Correspondence:* kahyo@hama-med.ac.jp

DOI: 10.1111/gtc.12092

2007). Such cell behaviors imply that the cells are alive and not dead. Unless escaping from a host cell, an internalized cell is eventually degraded through the autophagy-protein-dependent fusion of lysosomes to the vacuolar membranes surrounding the internalized cell (Florey *et al.* 2011). It has been reported that when a host cell enters mitosis with an internalized cell, the internalized cell can prevent the cytokinesis of the host cell, resulting in the generation of a binucleate cell, potentially contributing to aneuploidy (Krajcovic *et al.* 2011). Therefore, cell-in-cell structures may be one of the phenotypes representing some kind of genomic instability.

Although internalized cells inside host cells have been analyzed from the point of view of cell death, little is known about how and which cells, the engulfing host cells or the invading inhabitant cells, take the first initiative in the formation of the cell-in-cell structures. In this article, we report the establishment of a mutagenized cell line promoting the formation of cell-in-cell structures in the suspension culture condition. In this cell line, change in the culture condition reduced the frequency of formation of the cell-in-cell structures. Furthermore, the events of both engulfment and invasion involved in the formation of the cell-in-cell structures were promoted. This observation shows that the mutagenized cell line has the ability to exhibit both enhanced engulfment and enhanced invasion and suggests that the cellular environment has a key role in determining which of the two events, engulfment or invasion, predominates.

Results

Induction of cell-in-cell structures in the HCT116 cell line

Entosis is induced in the suspension culture condition and has been observed in various cell lines (Overholtzer *et al.* 2007). We had noticed, during the counting of a large number of the cells (Kahyo *et al.* 2011), that HCT116, a human colorectal cancer cell line, showed an extraordinarily small number of cell-in-cell structures on adhesive-coated culture dishes. Therefore, first of all, we examined the ability of HCT116 to form cell-in-cell structures under the suspension culture condition using a nonadhesive coating of the culture dishes (Fig. 1A). To avoid confusion, the word 'cell-in-cell' structures in this article is principally used for the nested doll-like structures, even if other words, such as entosis, may have been suitable. We counted the formation of both partial and complete forms, the former representing either the internalization or the extrusion process. The observations showed that the formation of both the partial and complete forms of the cell-in-cell structures was promoted in the suspension culture condition on a non-adhesive-coated surface. The number of cell-in-cell structures was increased by fivefold in suspension culture on a non-adhesive-coated culture dish (Student's *t*-test, $P = 0.005$). This result was consistent with a previous report on entosis (Overholtzer *et al.* 2007), which indicated that entosis of MCF10A and MCF7 cells occurred at a high frequency in suspension culture. However, in the HCT116 cell line, the cell-in-cell structures occurred at a frequency of approximately 1%, and the number of cell-in-cell structures was actually much smaller than that in the MCF7 cells (Fig. 1B; Student's *t*-test, $P < 0.001$).

Mutagenized cell line showing enhanced formation of cell-in-cell structures

The above observation suggests that an unknown mechanism suppresses the formation of cell-in-cell structures even under the suspension culture condition in the HCT116 cell line. Then, we attempted to boost the ability of the HCT116 cells to form cell-in-cell structures using the chemical mutagenesis method (Fig. 2A). HCT116 cells were treated for 8 h with ICR-191, an acridine derivative, which predominantly induced frameshift mutations (Cariello *et al.* 1990). ICR-191 was used at a concentration of 6.2 μg/mL, which killed half of the cells (Fig. S1 in Supporting Information). After colony formation, the colonies were picked up and cultured, and the cultured cells were distributed into two plates for subculture and cell-in-cell assay. In the assay for the cell-in-cell structures, the mutagenized cells were screened by microscopic observation. Four clones showing a relatively high frequency of cell-in-cell structures were selected of 144 clones on the assay plate, and cell counting showed that the 9F clone showed the largest number of cell-in-cell structures among the four clones (Fig. 2B). The 9F clone was amplified from the subculture plate and used for the second round of screening with ICR-191. Five clones with a relatively high frequency of cell-in-cell structures were selected of 144 single cell colonies from 9F clone. Finally, the cell clone, 9F-11A, which showed the highest ability to form cell-in-cell structures in the suspension culture condition, was

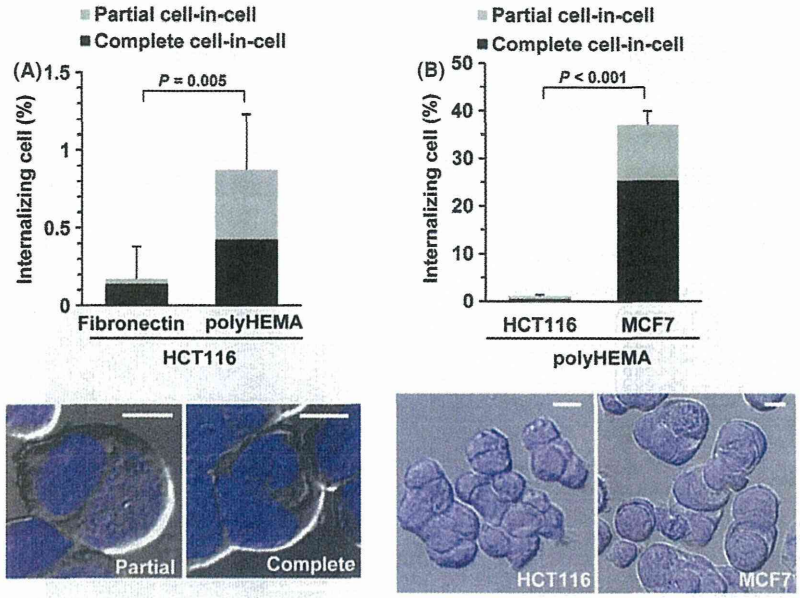

Figure 1 Cell-in-cell formation in the HCT116 cells. (A) HCT116 human colorectal cancer cells (12.5 cells/100 μm^2) were plated on to a fibronectin-coated (adhesive) or polyHEMA-coated (nonadhesive) dish and cultured for 14 h. The cells on the polyHEMA-coated dish were transferred on a silane-coated glass slip and centrifuged for attachment to the slip. The cells were fixed with paraformaldehyde and stained with DAPI. Cell-in-cell structures were observed and counted using differential interference contrast (DIC) optics and confocal laser scanning. (B) HCT116 cells (12.5 cells/100 μm^2) and MCF7 human breast cancer cells (8 cells/100 μm^2) were plated on to polyHEMA-coated dish and cultured for 14 h. The panels on the bottom are the images of representative cell-in-cell structures. Bar = 10 μm. The numbers of cells count in five (A) or six (B) experiments were as follows (cell-in-cell/total): 5/2697 (fibronectin) and 16/1792 (polyHEMA) in (A); and 35/3099 (HCT116) and 1118/3022 (MCF7) in (B). Data represent the mean ± SD of the total rate of complete and partial cell-in-cell structures.

acquired (Figs. 2B and 2C). 9F-11A showed a more than 10-fold higher number of cell-in-cell structures as compared to the parent HCT116 cells, and it was actually observed that the host cells contained whole cell bodies (Fig. 2D, left panel). Furthermore, time-lapse imaging analysis indicated that the internalized cells probably remained alive in the host cells for at least several hours (Fig. 2E, and Movie S1 in Supporting Information). Thus, the cell clone, 9F-11A, showing enhanced formation of the cell-in-cell structures, was generated from the HCT116 cell lines by the chemical mutagenesis method.

Culture conditions affecting the formation of the cell-in-cell structures in 9F-11A

On the cell-attachment dishes, the 9F-11A cells often showed different cell shapes as compared to the parent cells (Fig. 3A). Some 9F-11A cells extended slender pseudopodia, the lengths of which were sometimes twice to three times the sizes of the cell bodies themselves, whereas the parent cells rarely showed these features. As the altered regulation of actin polymerization was expected in the 9F-11A cells, the cell-in-cell assay using cytochalasin B (CytB), which is an inhibitor of actin polymerization and has been shown to be involved in the process of formation of the cell-in-cell structures (Lugini *et al.* 2006; Takeuchi *et al.* 2010), was carried out. The rate of the cell-in-cell structures was significantly lower in the CytB-treated cells than in the cells without the treatment of CytB (Fig. 3B; Student's *t*-test, $P = 0.002$ in the samples of 0.2 and 0.8 μg/mL of CytB). This result shows that the actin polymerization pathway is involved in the process of formation of the cell-in-cell structures in the 9F-11A cells. In contrast, similar to the case for the parent cell line, formation of the cell-in-cell structures in 9F-11A seemed to be suppressed on adhesive-coated dishes. Then, we examined the culture condition that would prevent the formation of cell-in-cell structures in 9F-11A, because the presence of cell-in-cell structures at a high frequency can cause genomic instability of the host cells, and we needed to subculture the 9F-11A